CK-666 and CK-869 differentially inhibit Arp2/3 iso-complexes

LuYan Cao[1, #], Shaina Huang[1], Angika Basant[1], Miroslav Mladenov[1] & Michael Way[1,2, #].

[1]The Francis Crick Institute, London, UK.

[2]Department of Infectious Disease, Imperial College, London, UK.

[#.] To whom correspondence should be addressed: luyan.cao@crick.ac.uk and michael.way@crick.ac.uk

Abstract

The inhibitors, CK-666 and CK-869, are widely used to probe the function of actin nucleation by the Arp2/3 complex *in vitro* and in cells. However, in mammals, the Arp2/3 complex consists of 8 iso-complexes, as three of its subunits (Arp3, ArpC1, ArpC5) are encoded by two different genes. Here, we used recombinant complexes with defined subunit composition to assess the activity of CK-666 and CK-869 against iso-complexes. We demonstrate that while both inhibitors prevent linear actin filament formation when either ArpC1A- or ArpC1B-containing complexes are activated by SPIN90, inhibition of actin branching depends on iso-complex composition. Both drugs inhibited actin branch formation by VCA-activated complexes containing ArpC1A, but only CK-869 can inhibit ArpC1B-containing complexes. Consistent with this, in bone marrow-derived macrophages which express very low levels of ArpC1A, CK-869 but not CK-666, impacted phagocytosis and migration. We also found that CK-869 is only able to inhibit Arp3- but not Arp3B-containing iso-complexes. Our analyses have important implications for the interpretation of results using CK-666 and CK-869, given that the relative expression levels of ArpC1 and Arp3 isoforms in cells and tissues remains largely unknown.

Introduction

The Arp2/3 complex is an important evolutionarily conserved nucleator of actin filaments (Machesky *et al*, 1997; Papalazarou & Machesky, 2021; Welch *et al*, 1997). The complex regulates the architecture and dynamics of actin cytoskeleton by initiating the formation of both branched and linear actin filaments (Espinoza-Sanchez *et al*, 2018; Gautreau *et al*, 2022; Mullins *et al*, 1998; Wagner *et al*, 2013). When activated by class I nucleating promoting factors (NPFs), such as WAVE, N-WASP and WASH, the Arp2/3 complex binds to the side of a pre-existing (mother) actin filament and nucleates the formation of a new (daughter) actin branch (Espinoza-Sanchez *et al.*, 2018; Molinie & Gautreau, 2018; Smith *et al*, 2013). Alternatively, Arp2/3 activation by SPIN90 (also known as WISH, NCKIPSD, Dip1) inhibits the association of the complex with an existing actin filament and generates a new linear actin filament (Luan *et al*, 2018; Wagner *et al.*, 2013). Through these two activities, the Arp2/3 complex plays essential roles in various cell processes, including endocytosis, cell migration, regulation of the actin cortex and DNA repair (Cao *et al*, 2020; Hinze & Boucrot, 2018; Papalazarou & Machesky, 2021; Schrank *et al*, 2018; Wu *et al*, 2012).

The Arp2/3 complex consists of seven subunits, including two Actin Related Proteins: Arp2, Arp3 and ArpC1-ArpC5. Upon activation by class I NPFs, the ArpC1-5 subunits interact with the mother actin filament while Arp2 and Arp3 act as a template to nucleate a new daughter filament (Chou *et al*, 2022; Ding *et al*, 2022; Fassler *et al*, 2020). In mammals but not lower eukaryotes, such as yeast and amoeba, Arp3, ArpC1 and ArpC5 exist as two different isoforms that are encoded by separate genes (Balasubramanian *et al*, 1996; Jay *et al*, 2000; Millard *et al*, 2003). In humans, Arp3 and Arp3B, ArpC1A and ArpC1B, ArpC5 and ArpC5L are 91, 67 and 67% identical respectively (Abella *et al*, 2016). Hence, in mammals, Arp2/3 complex is not a single species but a group of eight different iso-complexes. Moreover, these iso-complexes have different molecular properties as Arp2/3 complexes containing ArpC1B and ArpC5L are significantly better at stimulating actin assembly than those with ArpC1A and ArpC5 (Abella *et al.*, 2016), while actin networks assembled by Arp3B complexes disassemble faster than those formed by Arp3 complexes (Galloni *et al*, 2021). Structural analysis reveals that the higher branching efficiency of ArpC5L complexes is mediated by its disordered N-terminus (von Loeffelholz *et al*, 2020). Not surprisingly given their different properties, Arp2/3 iso-complexes have different cellular functions (Fassler *et al*, 2023; Molinie *et al*, 2019; Roman *et al*, 2017; Sadhu *et al*, 2023). The importance of Arp2/3 iso-complexes in cell and tissue homeostasis is also underscored by the observation that loss of function mutations in human ArpC1B lead to severe inflammation and immunodeficiency (Brigida *et al*, 2018; Kahr *et al*, 2017; Kuijpers *et al*, 2017; Randzavola *et al*, 2019; Somech *et al*, 2017; Volpi *et al*, 2019). It has also recently been reported that loss of ArpC5 expression results in multiple congenital

anomalies, recurrent infections, systemic inflammation, and mortality (Nunes-Santos *et al*, 2023; Sindram *et al*, 2023).

CK-666 and CK-869 are widely used as chemical inhibitors to probe the function of Arp2/3 complex in biochemical assays, cells and tissues (Nolen *et al*, 2009; Rotty *et al*, 2013; Yang *et al*, 2012). CK-666 binds between Arp2 and Arp3 to block the movement of these two subunits, which is required for activation of the Arp2/3 complex (Baggett *et al*, 2012; Hetrick *et al*, 2013; Rouiller *et al*, 2008). CK-869 inhibits this activating conformational change by binding to a hydrophobic pocket in Arp3 (Hetrick *et al.*, 2013). CK-869 has also been reported to inhibit microtubule assembly *in vitro* and cells (Yamagishi *et al*, 2018). Taking their different properties into consideration, we wondered whether all Arp2/3 iso-complexes can be inhibited by CK-666 and CK-869. In addition, it also remains to be established whether both drugs are equally effective against class 1 NPF- and SPIN90- mediated activation of Arp2/3 iso-complexes. To address these questions, we performed *in vitro* pyrene and TIRF assays, to examine the impact of CK-666 and CK-869 on the ability of defined recombinant Arp2/3 iso-complexes to nucleate actin when activated by the VCA domain of N-WASP or SPIN90. We found that the ability of CK-666 and CK-869 to inhibit Arp2/3 iso-complexes depends on their subunit composition and activation mechanism. Our observations have important implications for the interpretation of results from experiments using CK666 and CK869 to inhibit the function of the mammalian Arp2/3 complex both in cells and using purified complexes with unknown isoform composition. They also provide insights into the differences of Arp2/3 iso-complex activation by VCA domains and SPIN90.

Results and discussion

CK-869, but not CK-666, fully inhibits Vaccinia-induced actin polymerisation

We previously took advantage of Arp2/3 driven actin-based motility of vaccinia (Cudmore *et al*, 1996; Frischknecht *et al*, 1999; Leite & Way, 2015) as a model system to investigate whether Arp2/3 iso-complexes have different cellular activities (Abella *et al.*, 2016; Galloni *et al.*, 2021). We decided to use the same model to examine whether CK-666 and CK-869 differentially impact the ability of the vaccinia to promote branched actin network assembly. Examination of the literature reveals that these drugs are typically used at 100 μM in cell-based assays. Given this, we treated vaccinia infected HeLa cells 8 hours post infection with 50, 100, 200 and 300 μM CK-666 or CK-869 for 60 minutes and examined the localisation of cortactin as a specific marker for branched actin (Figure 1A). We found that while increasing doses of CK-869 result in a near-complete loss of virus induced actin assembly, CK-666 did not abolish actin polymerisation. Even at 300 μM, the number of virus-induced actin polymerisation events were not diminished (Figure 1B, C). The ability of vaccinia to stimulate

actin polymerization depends on their microtubule transport to the cell periphery and fusion with the plasma membrane (Hollinshead *et al*, 2001; Leite & Way, 2015; Newsome *et al*, 2004; Rietdorf *et al*, 2001). The inhibitory effect of CK-869 on actin assembly, however, was not the consequence of the lack of the virus reaching the plasma membrane as extracellular virions were readily detected on the outside of the cell (Figure 1B). Our observations on vaccinia infected HeLa cells demonstrate that CK-666 and CK-869 do not have the same impact on Arp2/3 driven actin assembly.

CK-666 does not inhibit ArpC1B-containing Arp2/3 complexes

It is not straightforward to deconvolve results from vaccinia infected cells as the precise levels of the 8 different Arp2/3 iso-complexes are not known in HeLa cells. We therefore decided to examine the impact of the two inhibitors using *in vitro* pyrene actin polymerisation assays with defined recombinant Arp2/3 complexes activated by GST-N-WASP-VCA. We initially used Arp2/3 iso-complexes containing Arp3 as it is 91% identical and much more abundant than Arp3B in most cells and tissues (Galloni *et al.*, 2021). We found that CK-869 but not CK-666 can inhibit ArpC1B containing Arp2/3 complexes with ArpC5 or ArpC5L (Figure 2A). This is unexpected given that CK-666 binds between Arp2 and Arp3 to block their movement during Arp2/3 complex activation (Baggett *et al*, 2012; Hetrick *et al*, 2013; Rouiller *et al*, 2008). To quantify actin branch initiation efficiency, we performed TIRF assays where the generation of new branches is observed over time by incubating fluorescent actin filaments with G-actin labelled with a different fluorophore (Risca *et al*, 2012). We found that ArpC1B/C5 generate actin branches at a rate 0.0022 ± 0.0007 μm^{-1} s^{-1} and 0.0025 ± 0.0007 μm^{-1} s^{-1} in the absence or presence of CK-666 respectively (Figure 2B). Similarly, ArpC1B/C5L generate actin branches at the same rate with (0.0032 ± 0.00005 μm^{-1} s^{-1}) or without CK-666 (0.0031 ± 0.0004 μm^{-1} s^{-1}). In contrast, CK-869 significantly reduces the branch generation rate of both ArpC1B/C5 and ArpC1B/C5L to 0.00005 ± 0.00001 μm^{-1} s^{-1} and 0.0003 ± 0.0002 μm^{-1} s^{-1} respectively (Figure 2B).

When we examined the effect of the drugs on ArpC1A containing Arp2/3 complexes in pyrene assays, we observed that both CK-666 and CK-869 slow down the actin polymerisation mediated by ArpC1A/C5 or ArpC1A/C5L containing complexes (Figure 3A). Quantification of TIRF assays reveals that CK-666 inhibits the branch generation rate of ArpC1A/C5 (0.0024 ± 0.0002 μm^{-1} s^{-1} to 0.0003 ± 0.0002 μm^{-1} s^{-1}) and ArpC1A/C5L (0.0026 ± 0.0006 μm^{-1} s^{-1} to 0.0002 ± 0.0001 μm^{-1} s^{-1}) containing complexes (Figure 3B). Similarly, CK-869 also reduces the branching rate of ArpC1A/C5 and ArpC1A/C5L containing complexes to 0.0001 ± 0.00005 μm^{-1} s^{-1} and 0.0001 ± 0.00002 μm^{-1} s^{-1} respectively (Figure 3B). Our results clearly demonstrate that CK-666 inhibits ArpC1A but not ArpC1B containing Arp2/3 complexes from generating

actin branches, whereas CK-869 inhibits both ArpC1 iso-complexes. Furthermore, the ArpC5/ArpC5L isoforms are not differentially impacted by either CK-666 or CK-869. The
150 results from our *in vitro* assays offer an explanation why CK-666 does not suppress vaccinia induced actin polymerization in HeLa cells, which express ~ 2.3 times as much ArpC1B as ArpC1A (Abella *et al.*, 2016).

CK-666 has no impact on macrophage phagocytosis and motility

155 Single-cell transcriptomics, tissue specific mRNA expression and proteomic analysis indicate that ArpC1B is highly expressed in immune cells compared to ArpC1A (Kahr *et al.*, 2017; Karlsson *et al*, 2021; Kim *et al*, 2014; Wu *et al*, 2009). Given this, we predicted that in contrast to CK-869, CK-666 will have little or no effect on Arp2/3 complex dependent activities in immune cells. After incubating murine bone marrow-derived macrophages with 100 μM of
160 Arp2/3 inhibitor, we observed that the morphology of macrophages treated with CK-869 changed significantly, with cells rounding up to become less spread (Figure 4A, B). In contrast, CK-666 treated macrophages were indistinguishable from DMSO treated controls. In addition, treatment with CK-666 had no impact on macrophage motility (Figure 4C). CK-869, on the other hand, increases macrophage movement. A similar increase in macrophage motility,
165 which is dependent on myosin II was observed in cells that contain no functional Arp2/3 complex as they lack ArpC2 (Rotty *et al*, 2017). The same study also found that the FcR phagocytic capability of CK-666 treated macrophages is similar to DMSO-treated controls. Extending this observation, we found that CK-869 but not CK-666 decreased the ability of macrophages to phagocytose zymosan compared to DMSO-treated controls (Figure 4D). Our
170 observations in macrophages indicate that the ability of CK-666 to inhibit Arp2/3 dependent processes will depend on the relative expression of ArpC1A compared to ArpC1B, which will vary across cell types and tissues.

CK-666 and CK-869 do not disrupt the Arp2/3 complex binding to F-actin or VCA

175 Structural data indicate that neither CK-666 nor CK-869 binds directly to the ArpC1 subunit (Nolen *et al.*, 2009). The divergent effects of CK-666 on ArpC1A and ArpC1B within the Arp2/3 complex remains enigmatic. A possible explanation may be that the drugs affect the interaction between Arp2/3 iso-complexes and actin filaments indirectly. To investigate this, we performed actin filament co-sedimentation assays using ArpC1A and ArpC1B-containing
180 complexes in the absence of VCA-mediated activation. We found that regardless of the presence of drugs, comparable quantities of ArpC1A and ArpC1B-containing Arp2/3 complexes co-pelleted with actin filaments (Figure 5A, B). This indicates that neither CK-666 nor CK-869 impairs the interaction between the Arp2/3 complex and actin filaments, in the context of different ArpC1 isoforms. Interestingly, the level of ArpC1B/C5L co-pelleting with

185 actin is a nearly twofold greater than complexes containing ArpC1A/C5L (Figure. 5A, B). This may in part explain why Arp2/3 complex with ArpC1B/C5L is a more efficient branch generator than those with ArpC1A/C5L (Figure. 2B, 3B) (Abella *et al.*, 2016).

Previous observations indicate that CK-666 and CK-869 do not impact VCA binding (Hetrick
190 *et al.*, 2013). However, in this study the Arp2/3 complex will be a mixture of iso-complexes as it was isolated from bovine brain (Abella *et al.*, 2016). We therefore performed GST-N-WASP-VCA pulldown assays to capture ArpC1A and ArpC1B containing complexes in the presence or absence of Arp2/3 inhibitors to examine if there are iso-complex specific differences. We found that the presence of either drug did not alter the quantity of ArpC1A- and ArpC1B-
195 containing Arp2/3 complexes bound to GST-N-WASP-VCA (Figure 5C). These results are consistent with previous observations, irrespective of the presence of distinct ArpC1 isoforms (Hetrick *et al.*, 2013). It also suggests that inhibited and uninhibited Arp2/3 iso-complexes will compete for VCA binding in cells, which has important implications depending on the relative levels of ArpC1A and ArpC1B containing complexes and which inhibitor is used.

200

CK-666 inhibits activation of all Arp2/3 iso-complexes by SPIN90.

As CK-666 can prevent ArpC1A, but not ArpC1B, containing Arp2/3 complexes from generating VCA-dependent actin branches, we decided to investigate whether the same is true when Arp2/3 is activated to form linear actin filaments by SPIN90. Pyrene assays
205 demonstrate that CK-666 and CK-869 inhibit SPIN90-dependent actin polymerisation irrespective of the ArpC1 isoform (Figure 6A). We also observed by TIRF microscopy that both drugs inhibit actin filament formation by ArpC1A and ArpC1B containing complexes (Fig. 6B). In contrast to the pyrene actin polymerisation experiments, which are an indirect bulk assay, the TIRF assays also revealed that CK-869 is a more potent inhibitor than CK-666.

210

We then performed GST pull down assays to investigate if CK-666 or CK-869 prevent Arp2/3 from binding to SPIN90 (Figure 6C). Neither drug inhibited the interaction of Arp2/3 with SPIN90. However, unexpectedly CK-869 promotes the binding of Arp2/3 to SPIN90, with the interaction with ArpC1A and ArpC1B containing complexes increasing ~15- and 5-fold
215 respectively. There was also a slight increase in binding in the presence of CK-666. A possible explanation is that CK-869 blocks the Arp2/3 complex in an inactive state which favours its binding to SPIN90 but prevents further conformational changes required for full activation which weaken the association with SPIN90. This would imply that inactive Arp2/3 has a higher affinity for SPIN90 than the active complex as is observed for VCA but not
220 cortactin NtA (Liu *et al*, 2023; Zimmet *et al*, 2020). This may explain why the amount of Arp2/3

pulled down with GST-SPIN90 is reduced in the presence of GST-N-WASP-VCA (Cao *et al*, 2023).

CK-869 cannot inhibit Arp3B-containing complexes

Our results thus far demonstrate that CK-869 is a better inhibitor of Arp3-containing complexes than CK-666. To explore whether the same is also true for Arp3B containing complexes, we purified Arp2/3 complex containing Arp3B, ArpC1B and ArpC5L and examined the impact of both inhibitors on the ability of the complex to nucleate actin filaments. Quantification of actin assembly in TIRF assays reveals that the branching rates induced by GST-N-WASP-VCA in the presence of CK-666 or CK-869 were indistinguishable from DMSO-treated controls (Figure 7A). The activity of CK-666 is consistent with our earlier observation that the drug cannot inhibit ArpC1B containing complexes in an Arp3 background (Figure 2A, B). However unexpectedly, CK-869 has a different activity towards Arp3B and Arp3 containing complexes. Next, we tested whether both drugs inhibit SPIN90 mediated activation of Arp3B-containing complexes. As observed with Arp3-containing complexes (Figure 6B), CK-666 also inhibits the ability of SPIN90 to stimulate linear actin filament assembly by Arp3B-containing complexes (Figure 7B). In sharp contrast, Arp3B-containing complexes efficiently generate linear actin filaments in the presence of CK-869 (Figure 7B). Our *in vitro* data demonstrate that CK-869 cannot inhibit Arp3B-containing complexes.

Previous structural analysis reveals that CK-666 interacts mostly with Arp2 but forms two hydrophobic interactions with leucine 117 and threonine 119 of Arp3 (Baggett *et al.*, 2012). These two residues are conserved in Arp3B, suggesting that the binding of CK-666 will be similar, which is consistent with our in vitro data. In contrast, several residues in the hydrophobic CK-869 binding pocket of Arp3 differ to those in Arp3B (Hetrick *et al.*, 2013) (Figure 7C). Notably, the leucine 126 (Leu 126) in Arp3B may have direct clashes with CK-869 and preclude its binding leading to a loss of inhibition. Interestingly, CK-869 does not inhibit Arp2/3 in budding and fission yeast due to non-conserved residues in the CK-869 binding pocket (Nolen *et al.*, 2009).

Conclusions

Using purified components and *in vitro* assays we have demonstrated that CK-666 can inhibit the formation of SPIN90-induced linear actin filaments by all Arp2/3 iso-complexes, however, it fails to suppress the initiation of actin branch formation by complexes containing ArpC1B. In contrast, CK-869 prevents Arp3- but not Arp3B-containing complexes from generating both actin branches and linear actin filaments. Our results provide further evidence that Arp2/3 iso-complexes have different molecular properties. This observation also aligns with our cellular

findings, where CK-869 exhibited greater efficacy in inhibiting vaccinia-induced actin networks compared to CK-666. Examination of the literature reveals that most studies typically treat cells with CK-666 rather than CK-869, presumably because the latter is more toxic as it will result in complete loss of Arp2/3 function.

Our study highlights the distinct impact of CK-666 and CK-869 on Arp2/3 complexes, depending on whether they are activated by VCA or SPIN90. The observation that CK-666 has no discernible effect on the binding of Arp2/3 to either NPF I or mother filaments indicates that CK-666 primarily disrupts the conformational changes of Arp2 and Arp3 to prevent the complex activated states as suggested by the previous structural data (Baggett *et al.*, 2012). The ability of ArpC1B-containing complexes to generate actin branches in the presence of CK-666 underscores their robust adaptability to the activated conformation induced by NPF I. Conversely, both drugs can effectively inhibit Arp2/3-SPIN90 generating actin filaments, while simultaneously enhancing, to varying degrees, the binding of Arp2/3 complexes to SPIN90. This implies that SPIN90 may induce a relatively weak activation of Arp2/3 complexes, which is more susceptible to inhibition.

The pivotal role of Arp2/3 complexes in many cellular processes that can become dysregulated in pathological conditions, highlights the ongoing need to screen for additional Arp2/3 inhibitors. Suppressing cancer cell migration and tumour metastasis, two ArpC2 binding inhibitors, were recently identified by revisiting FDA-approved drugs (Choi *et al*, 2019; Yoon *et al*, 2019). Several CK-666 structural analogues have been reported to have inhibitory effect on the Arp2/3 complex and two of them have better *in vivo* efficiency compared with CK-666 (Fokin *et al*, 2022). Given our results, it is possible that these drugs have different inhibitory effects on Arp2/3 iso-complexes. In summary, our results have important implications for the interpretation of experiments with CK-666 and CK-869 but also illuminate the potential utility of these inhibitors in exploring the cellular functions of specific Arp2/3 iso-complexes.

295 **Materials and methods**

Vaccinia virus infection and drug treatment

HeLa cells plated on fibronectin-coated coverslips were infected with Western Reserve Vaccinia virus in serum-free Minimum Essential Medium (MEM) at multiplicity of infection (MOI) = 2 (Frischknecht *et al.*, 1999). After one hour at 37°C, the serum-free MEM was removed and
300 replaced with complete MEM. At 8 hours post-infection, media was replaced with complete MEM containing CK-666 (Sigma, SML0006-5MG) or CK-869 (Sigma, C9124-5MG) or DMSO at desired concentrations for 1 hour prior to fixation.

Immunofluorescence and actin tail quantification

305 As previously described (Basant & Way, 2022), cells were fixed with 4% paraformaldehyde in PBS for 10 min, blocked in cytoskeletal buffer (1 mM MES, 15 mM NaCl, 0.5 mM EGTA, 0.5 mM $MgCl_2$, and 0.5 mM glucose, pH 6.1) containing 2% (vol/vol) fetal calf serum and 1% (wt/vol) BSA for 30 min. To visualize extra-cellular vaccinia virus particles, prior to permeabilization with detergent, the cells were stained with a monoclonal antibody against B5
310 (19C2, rat, 1:1000 (Schmelz *et al*, 1994)) followed by an Alexa Fluor 647 anti-rat secondary antibody (Invitrogen; 1:1000 in blocking buffer). Cells were then permeabilized with 0.1% Triton-X/PBS for 3 min. Branched actin was labelled with cortactin monoclonal antibody (Millipore (p80/85); 1:400), followed by Alexa Fluor 488 conjugated secondary antibody (Invitrogen; 1:1000 in blocking buffer). Actin filaments were labelled with Alexa Fluor 568
315 phalloidin (Invitrogen; 1:500). Coverslips were mounted on glass slides using Mowiol (Sigma) and imaged on a Zeiss Axioplan2 microscope equipped with a 63x/1.4 NA. Plan-Achromat objective and a Photometrics Cool Snap HQ cooled charge-coupled device camera. The microscope was controlled with MetaMorph 7.8.13.0 software.

320 *Bone marrow-derived macrophage migration and phagocytosis*

All animal work was authorized by UK Home Office project license P7E080263 and personal licenses following the approval by the Animal Welfare and Ethical Review Body of The Francis Crick Institute. Murine bone marrow was extracted from tibia and femur of C57BL/6Jax mice and differentiated *in vitro* for 7 days in macrophage conditional medium (RPMI supplemented
325 with 30% L929 conditioned medium, 20% FBS and 1% P/S) to obtain bone marrow-derived macrophages (BMDM).

To examine the effects of different inhibitors on cell morphology and migration, BMDM were seeded in 24-well glass bottomed plates (Cellvis) at $1*10^4$ cells/well in 500 µL of macrophage
330 conditional medium. Cells were imaged and analyzed using the Livecyte system (Phasefocus) every 10 mins for 24 h at 10 x with two fields of view per well. The imaging chamber was

maintained at 37°C with 5% CO_2. Meanwhile, cells were seeded at 2 *10^4 cells/well in Glass-bottomed 8-well µ-Slides (ibidi) and imaged using an inverted widefield Nikon Ti2 Eclipse long-term time lapse system with an LED illumination system. The imaging chamber was maintained at 37°C with 5% CO_2. A Nikon 20× Ph2 planar (plan) apochromatic (apo) (0.75 N.A.) air objective was used to acquire images at a single *z*-slice every 10 min for 5 hours with two fields of view per well.

To assess the effects of different inhibitors on phagocytosis, BMDM were seeded in 96-well V-bottom plates (Corning) at 1*10^5 cells/well in 100 µL macrophage conditional medium supplemented with different inhibitors or DMSO as indicated. BMDM were incubated with 25 µg/mL pHrodo zymosan bio-particles (Invitrogen) for up to 120 min at 37ºC, 5% CO_2. Cells were then washed with PBS and stained with an antibody cocktail (Live/Dead Fixable Violet Dead Cell Stain (1:500, Invitrogen), CD11b-BV711 (1:100, BioLegend), F4/80-APC (1:100, eBiosciences)) to identify the live BMDM. Samples were then assessed by flow cytometry and the phagocytic fraction indicated the % of *(BMDM internalized the zymosan bio-particles) / (Total BMDM)*.

Protein purification and preparation

GST-tagged human N-WASP-VCA (392 – 505, UniProt O00401), human SPIN90 C-terminus (267 - 715, UniProt Q9NZQ3-3), were purified following the previously reported protocols (Cao *et al.*, 2023). Recombinant human Arp2/3 iso-complexes with defined composition (Uniprot P61160, P61158, Q9P1U1, Q92747, O15143, O15144, O15145, P59998, Q9H9F9, Q98PX5) were purified following the previously reported protocol (Baldauf *et al*, 2023). Skeletal muscle alpha-actin was purified from rabbit muscle atone powder following the published protocol (Spudich & Watt, 1971). Actin was fluorescently labelled on the surface lysine 328, using Alexa-488 or Alexa-594 succinimidyl ester (Life Technologies) as previously reported protocol (Romet-Lemonne *et al*, 2018). Pyrenyl-actin was made by labelling actin with N(1-pyrene)-iodoacetamide (Thermo Fisher Scientific) (Cooper *et al*, 1983).

To mimic the use of drugs in cells, Arp2/3 iso-complex was incubated with 100 µM CK-666 or CK-869 (Sigma, Bio-Techne), or equivalent amount of DMSO at room temperature for 1 hour before being added to the experimental system.

Pyrene actin polymerisation assay

Actin polymerisation induced by Arp2/3 and NPF I is very fast. To have a good resolution, 2 nM Arp2/3 iso-complexes, 5 nM GST-N-WASP-VCA and 2 µM G-actin (5% pyrene labelled) was mixed and measured in a Safas Xenius fluorimeter at room temperature (von Loeffelholz

et al., 2020). The negative control experiment was done without GST-N-WASP-VCA. For
370 experiments with SPIN90, the same concentration of Arp2/3 iso-complexes was used together with 100 nM SPIN90-Cter and 2.5 μM G-actin (5% pyrene labelled). The negative control for these experiments lacked SPIN90-Cter. All actin assembly assays were performed in a buffer containing 5 mM Tris HCl pH 7.0, 50 mM KCl, 0.2 mM ATP, 1 mM $MgCl_2$, 1 mM EGTA and 1 mM DTT in addition to 100 μM CK-666 or CK-869 or equivalent amount of DMSO.
375

TIRF assays

Deep UV treated coverslips were passivated by mPEG silane overnight. The coverslips were rinsed thoroughly with ethanol and water. Before experiments, dried coverslips were stuck to the glass slides with 3 mm-separated parafilm bands to create flow chambers. The
380 experiments were performed in TIRF buffer: 5 mM Tris HCl pH 7.0, 50 mM KCl, 1 mM $MgCl_2$, 0.2 mM EGTA, 0.2 mM ATP, 10 mM DTT, 1 mM DABCO, 0.1% BSA and 0.3% Methylcellulose 4000 cP at 25 °C.

Actin branching assays were performed as previously described (Cao *et al.*, 2020). To quantify
385 the branching efficiency, 2.5 μM G-actin (15% Alexa-488 labelled) was pre-incubated in experimental buffer at room temperature for 1 hour to form fluorescent actin filaments. During experiment, 25 nM pre-polymerised actin (15% Alexa-488 labelled) was mixed with 50 nM GST-N-WASP-VCA, 0.5 μM profilin, 10 nM of 1 hour inhibitor-treated Arp2/3 in addition to 100 μM CK-666 or CK-869 (final concentration) or equivalent amount of DMSO. G-actin (0.5 μM,
390 15 % Alexa-568 labelled) was added to the system at the last moment. Then the mixture was immediately flowed into the chamber for imaging. The moment when G-actin added into the system was recorded as time 0. Branch generation was observed over time. The number of branches generated per μm of actin filaments per minute was quantified as the branching rate. To study the actin nucleation by SPIN90, the 50 nM GST-N-WASP-VCA was replaced 200
395 nM SPIN90-Cter and 20 nM of inhibitor treated Arp2/3 were used as in the same protocol as above.

GST pull down assays

Prior to performing pull-down assays, the Glutathione Sepharose™ 4B resin (GE Healthcare)
400 was incubated with 5% BSA for 5 minutes and washed 3 times with GST pull-down buffer containing 50 mM Tris-HCl pH 7.0, 1 mM $MgCl_2$, 0.2 mM EGTA, 0.2 mM ATP, 1 mM DTT, 50 mM KCl, and 5% glycerol. Glutathione Sepharose 4B beads were mixed with 50 μL of 5 μM GST-SPIN90-Cter or GST-N-WASP-VCA, 200 nM drug treated Arp2/3 in addition to 100 μM inhibitor or equivalent amount of DMSO. After 1 hour incubation at room temperature, the resin
405 was then washed 3 times with 300 μL of GST pull-down buffer. The proteins bound to the

resin were eluted with 50 µL of 50 mM GSH (reduced glutathione). The sample was analysed by SDS-PAGE followed by western blot using Anti-ArpC2 (Sigma) to detect Arp2/3 complexes. Amersham imager AI600 was used to develop the western blot results. The amount of GST-tagged protein eluted from the resin was detected by ponceau. The negative control experiment was done in the same way except 50 µL of 5 µM Glutathione Sepharose™ 4B attached GST was used instead of GST-SPIN90-Cter or GST-N-WASP-VCA.

F-Actin co-sedimentation assay

G-actin (15 µM) was incubated in F-buffer (5 mM Tris pH 7.0, 100 mM KCl, 0.2 mM ATP, 1 mM $MgCl_2$, and 1 mM DTT) at room temperature for 1 hour before 7.5 µM of the polymerised actin filaments were mixed with 4 µM inhibitor treated Arp2/3 iso-complexes in F-buffer in the presence of 100 µM CK-666 or CK-869 or equivalent amount of DMSO at room temperature for 1 hour. The supernatant and pellet were then separated by ultracentrifuge at 70000 rpm at 25 °C for 30 minutes. Pellet was resuspended with 50 µL of F-buffer and the same amount (20 µL) of supernatant and pellet was loaded on a SDS page. The negative control only has Arp2/3 iso-complexes without F-actin.

Image analysis and quantitation

Fiji software was used to analyse images, western blots and Coomassie blue gels manually (Schindelin *et al*, 2012). Quantification of branched actin induced by vaccinia virus was performed using two-colour fixed cell images where cortactin and extracellular virus were labelled. Ten images were analysed per condition in three independent experiments. In each image 10-15 isolated extracellular virus particles were blindly selected and the presence of associated cortactin was determined in the corresponding channel for a total of ~ 400 virus particles.

Actin branching rate in TIRF assay was quantified by counting the number of generated branches per µm length of actin mother filament per second. In each condition, the ten longest mother filaments were chosen to analyse. Three independent repeats were performed. Actin nucleation by SPIN90-Arp2/3 complex in TIRF assay was quantified by measuring the filament density of a randomly picked field of view (59 µm x 59 µm) at 240s. Three independent repeats were performed.

Livecyte automatically quantified the motility and the morphology of macrophages by measuring their moving speed as well as their thickness and their length/width ratio. For each condition, more than 30 cells were quantified. The experiments were repeated five times independently.

Protein structure analysis

Pymol is used to visualize and analyse the structure of drug bound Arp2/3 complex (Schrodinger, 2010). Potential Van-der-Waals clashes were detected by show_bumps plugin.

Acknowledgements

This project has received funding from the European Research Council (ERC) under the European Union's Horizon 2020 research and innovation programme (grant agreement No 810207 to Michael Way. Luyan Cao was supported by the European Union's Horizon 2020 Marie Sklodowka-Curie individual fellowship program (H2020-MSCA-IF-101028239 – MolecularArp) and the ERC Synergy grant (No 810207). MW is additionally supported by the Francis Crick Institute, which receives its core funding from Cancer Research UK (CC2096), the UK Medical Research Council (CC2096), and the Wellcome Trust (CC2096). We Carolyn Moores (Birkbeck, University of London), Snezhka Oliferenko & Jeremy Carlton (the Francis Crick Institute, London) and Antoine Jegou (Institut Jacques Monod, Paris) for feedback on the manuscript. For the purpose of Open Access, the authors have applied a CC BY public copyright licence to any Author Accepted Manuscript version arising from this submission.

References

Abella JV, Galloni C, Pernier J, Barry DJ, Kjaer S, Carlier MF, Way M (2016) Isoform diversity in the Arp2/3 complex determines actin filament dynamics. *Nat Cell Biol* 18: 76-86

Baggett AW, Cournia Z, Han MS, Patargias G, Glass AC, Liu SY, Nolen BJ (2012) Structural characterization and computer-aided optimization of a small-molecule inhibitor of the Arp2/3 complex, a key regulator of the actin cytoskeleton. *ChemMedChem* 7: 1286-1294

Balasubramanian MK, Feoktistova A, McCollum D, Gould KL (1996) Fission yeast Sop2p: a novel and evolutionarily conserved protein that interacts with Arp3p and modulates profilin function. *EMBO J* 15: 6426-6437

Baldauf L, Frey F, Perez MA, Mladenov M, Way M, Idema T, Koenderink GH (2023) Biomimetic actin cortices shape cell-sized lipid vesicles. *bioRxiv*: 2023.2001.2015.524117

Basant A, Way M (2022) The relative binding position of Nck and Grb2 adaptors impacts actin-based motility of Vaccinia virus. *Elife* 11

Brigida I, Zoccolillo M, Cicalese MP, Pfajfer L, Barzaghi F, Scala S, Oleaga-Quintas C, Alvarez-Alvarez JA, Sereni L, Giannelli S *et al* (2018) T-cell defects in patients with ARPC1B germline mutations account for combined immunodeficiency. *Blood* 132: 2362-2374

Cao L, Ghasemi F, Way M, Jegou A, Romet-Lemonne G (2023) Regulation of branched versus linear Arp2/3-generated actin filaments. *EMBO J* 42: e113008

Cao L, Yonis A, Vaghela M, Barriga EH, Chugh P, Smith MB, Maufront J, Lavoie G, Meant A, Ferber E *et al* (2020) SPIN90 associates with mDia1 and the Arp2/3 complex to regulate cortical actin organization. *Nat Cell Biol* 22: 803-814

Choi J, Lee YJ, Yoon YJ, Kim CH, Park SJ, Kim SY, Doo Kim N, Cho Han D, Kwon BM (2019) Pimozide suppresses cancer cell migration and tumor metastasis through binding to ARPC2, a subunit of the Arp2/3 complex. *Cancer Sci* 110: 3788-3801

Chou SZ, Chatterjee M, Pollard TD (2022) Mechanism of actin filament branch formation by Arp2/3 complex revealed by a high-resolution cryo-EM structureof the branch junction. *Proc Natl Acad Sci U S A* 119: e2206722119

Cooper JA, Walker SB, Pollard TD (1983) Pyrene actin: documentation of the validity of a sensitive assay for actin polymerization. *J Muscle Res Cell Motil* 4: 253-262

Cudmore S, Reckmann I, Griffiths G, Way M (1996) Vaccinia virus: a model system for actin-membrane interactions. *J Cell Sci* 109 (Pt 7): 1739-1747

Ding B, Narvaez-Ortiz HY, Singh Y, Hocky GM, Chowdhury S, Nolen BJ (2022) Structure of Arp2/3 complex at a branched actin filament junction resolved by single-particle cryo-electron microscopy. *Proc Natl Acad Sci U S A* 119: e2202723119

Espinoza-Sanchez S, Metskas LA, Chou SZ, Rhoades E, Pollard TD (2018) Conformational changes in Arp2/3 complex induced by ATP, WASp-VCA, and actin filaments. *Proc Natl Acad Sci U S A* 115: E8642-E8651

Fassler F, Dimchev G, Hodirnau VV, Wan W, Schur FKM (2020) Cryo-electron tomography structure of Arp2/3 complex in cells reveals new insights into the branch junction. *Nat Commun* 11: 6437

Fassler F, Javoor MG, Datler J, Doring H, Hofer FW, Dimchev G, Hodirnau VV, Faix J, Rottner K, Schur FKM (2023) ArpC5 isoforms regulate Arp2/3 complex-dependent protrusion through differential Ena/VASP positioning. *Sci Adv* 9: eadd6495

Fokin AI, Chuprov-Netochin RN, Malyshev AS, Romero S, Semenova MN, Konyushkin LD, Leonov SV, Semenov VV, Gautreau AM (2022) Synthesis, Screening and Characterization of Novel Potent Arp2/3 Inhibitory Compounds Analogous to CK-666. *Front Pharmacol* 13: 896994

Frischknecht F, Moreau V, Rottger S, Gonfloni S, Reckmann I, Superti-Furga G, Way M (1999) Actin-based motility of vaccinia virus mimics receptor tyrosine kinase signalling. *Nature* 401: 926-929

Galloni C, Carra D, Abella JVG, Kjaer S, Singaravelu P, Barry DJ, Kogata N, Guerin C, Blanchoin L, Way M (2021) MICAL2 enhances branched actin network disassembly by oxidizing Arp3B-containing Arp2/3 complexes. *J Cell Biol* 220

Gautreau AM, Fregoso FE, Simanov G, Dominguez R (2022) Nucleation, stabilization, and disassembly of branched actin networks. *Trends Cell Biol* 32: 421-432

Hetrick B, Han MS, Helgeson LA, Nolen BJ (2013) Small molecules CK-666 and CK-869 inhibit actin-related protein 2/3 complex by blocking an activating conformational change. *Chem Biol* 20: 701-712

Hinze C, Boucrot E (2018) Local actin polymerization during endocytic carrier formation. *Biochem Soc Trans* 46: 565-576

Hollinshead M, Rodger G, Van Eijl H, Law M, Hollinshead R, Vaux DJ, Smith GL (2001) Vaccinia virus utilizes microtubules for movement to the cell surface. *J Cell Biol* 154: 389-402

Jay P, Berge-Lefranc JL, Massacrier A, Roessler E, Wallis D, Muenke M, Gastaldi M, Taviaux S, Cau P, Berta P (2000) ARP3beta, the gene encoding a new human actin-related protein, is alternatively spliced and predominantly expressed in brain neuronal cells. *Eur J Biochem* 267: 2921-2928

Kahr WH, Pluthero FG, Elkadri A, Warner N, Drobac M, Chen CH, Lo RW, Li L, Li R, Li Q *et al* (2017) Loss of the Arp2/3 complex component ARPC1B causes platelet abnormalities and predisposes to inflammatory disease. *Nat Commun* 8: 14816

Karlsson M, Zhang C, Mear L, Zhong W, Digre A, Katona B, Sjostedt E, Butler L, Odeberg J, Dusart P *et al* (2021) A single-cell type transcriptomics map of human tissues. *Sci Adv* 7

Kim MS, Pinto SM, Getnet D, Nirujogi RS, Manda SS, Chaerkady R, Madugundu AK, Kelkar DS, Isserlin R, Jain S *et al* (2014) A draft map of the human proteome. *Nature* 509: 575-581

Kuijpers TW, Tool ATJ, van der Bijl I, de Boer M, van Houdt M, de Cuyper IM, Roos D, van Alphen F, van Leeuwen K, Cambridge EL *et al* (2017) Combined immunodeficiency with severe inflammation and allergy caused by ARPC1B deficiency. *J Allergy Clin Immunol* 140: 273-277 e210

Leite F, Way M (2015) The role of signalling and the cytoskeleton during Vaccinia Virus egress. *Virus Res* 209: 87-99

Liu T, Cao L, Mladenov M, Jegou A, Way M, Moores CA (2023) Cortactin stabilizes actin branches by bridging activated Arp2/3 to its nucleated actin filament. *bioRxiv*: 2023.2008.2016.553490

Luan Q, Liu SL, Helgeson LA, Nolen BJ (2018) Structure of the nucleation-promoting factor SPIN90 bound to the actin filament nucleator Arp2/3 complex. *EMBO J* 37

Machesky LM, Reeves E, Wientjes F, Mattheyse FJ, Grogan A, Totty NF, Burlingame AL, Hsuan JJ, Segal AW (1997) Mammalian actin-related protein 2/3 complex localizes to regions of lamellipodial protrusion and is composed of evolutionarily conserved proteins. *Biochem J* 328 : 105-112

Millard TH, Behrendt B, Launay S, Futterer K, Machesky LM (2003) Identification and characterisation of a novel human isoform of Arp2/3 complex subunit p16-ARC/ARPC5. *Cell Motil Cytoskeleton* 54: 81-90

Molinie N, Gautreau A (2018) The Arp2/3 Regulatory System and Its Deregulation in Cancer. *Physiol Rev* 98: 215-238

Molinie N, Rubtsova SN, Fokin A, Visweshwaran SP, Rocques N, Polesskaya A, Schnitzler A, Vacher S, Denisov EV, Tashireva LA *et al* (2019) Cortical branched actin determines cell cycle progression. *Cell Res* 29: 432-445

Mullins RD, Heuser JA, Pollard TD (1998) The interaction of Arp2/3 complex with actin: nucleation, high affinity pointed end capping, and formation of branching networks of filaments. *Proc Natl Acad Sci U S A* 95: 6181-6186

Newsome TP, Scaplehorn N, Way M (2004) SRC mediates a switch from microtubule- to actin-based motility of vaccinia virus. *Science* 306: 124-129

Nolen BJ, Tomasevic N, Russell A, Pierce DW, Jia Z, McCormick CD, Hartman J, Sakowicz R, Pollard TD (2009) Characterization of two classes of small molecule inhibitors of Arp2/3 complex. *Nature* 460: 1031-1034

Nunes-Santos CJ, Kuehn H, Boast B, Hwang S, Kuhns DB, Stoddard J, Niemela JE, Fink DL, Pittaluga S, Abu-Asab M *et al* (2023) Inherited ARPC5 mutations cause an actinopathy impairing cell motility and disrupting cytokine signaling. *Nat Commun* 14: 3708

Papalazarou V, Machesky LM (2021) The cell pushes back: The Arp2/3 complex is a key orchestrator of cellular responses to environmental forces. *Curr Opin Cell Biol* 68: 37-44

Randzavola LO, Strege K, Juzans M, Asano Y, Stinchcombe JC, Gawden-Bone CM, Seaman MN, Kuijpers TW, Griffiths GM (2019) Loss of ARPC1B impairs cytotoxic T lymphocyte maintenance and cytolytic activity. *J Clin Invest* 129: 5600-5614

Rietdorf J, Ploubidou A, Reckmann I, Holmstrom A, Frischknecht F, Zettl M, Zimmermann T, Way M (2001) Kinesin-dependent movement on microtubules precedes actin-based motility of vaccinia virus. *Nat Cell Biol* 3: 992-1000

Risca VI, Wang EB, Chaudhuri O, Chia JJ, Geissler PL, Fletcher DA (2012) Actin filament curvature biases branching direction. *Proc Natl Acad Sci U S A* 109: 2913-2918

Roman W, Martins JP, Carvalho FA, Voituriez R, Abella JVG, Santos NC, Cadot B, Way M, Gomes ER (2017) Myofibril contraction and crosslinking drive nuclear movement to the periphery of skeletal muscle. *Nat Cell Biol* 19: 1189-1201

Romet-Lemonne G, Guichard B, Jegou A (2018) Using Microfluidics Single Filament Assay to Study Formin Control of Actin Assembly. *Methods Mol Biol* 1805: 75-92

Rotty JD, Brighton HE, Craig SL, Asokan SB, Cheng N, Ting JP, Bear JE (2017) Arp2/3 Complex Is Required for Macrophage Integrin Functions but Is Dispensable for FcR Phagocytosis and In Vivo Motility. *Dev Cell* 42: 498-513 e496

Rotty JD, Wu C, Bear JE (2013) New insights into the regulation and cellular functions of the ARP2/3 complex. *Nat Rev Mol Cell Biol* 14: 7-12

Rouiller I, Xu XP, Amann KJ, Egile C, Nickell S, Nicastro D, Li R, Pollard TD, Volkmann N, Hanein D (2008) The structural basis of actin filament branching by the Arp2/3 complex. *J Cell Biol* 180: 887-895

Sadhu L, Tsopoulidis N, Hasanuzzaman M, Laketa V, Way M, Fackler OT (2023) ARPC5 isoforms
635 and their regulation by calcium-calmodulin-N-WASP drive distinct Arp2/3-dependent actin remodeling events in CD4 T cells. *Elife* 12

Schindelin J, Arganda-Carreras I, Frise E, Kaynig V, Longair M, Pietzsch T, Preibisch S, Rueden C, Saalfeld S, Schmid B *et al* (2012) Fiji: an open-source platform for biological-image analysis.
640 *Nat Methods* 9: 676-682

Schmelz M, Sodeik B, Ericsson M, Wolffe EJ, Shida H, Hiller G, Griffiths G (1994) Assembly of vaccinia virus: the second wrapping cisterna is derived from the trans Golgi network. *J Virol* 68: 130-147

645

Schrank BR, Aparicio T, Li Y, Chang W, Chait BT, Gundersen GG, Gottesman ME, Gautier J (2018) Nuclear ARP2/3 drives DNA break clustering for homology-directed repair. *Nature* 559: 61-66
Schrodinger, LLC, 2010. The PyMOL Molecular Graphics System, Version 1.3r1.

650 Sindram E, Caballero-Oteyza A, Kogata N, Chor Mei Huang S, Alizadeh Z, Gamez-Diaz L, Fazlollhi MR, Peng X, Grimbacher B, Way M *et al* (2023) ARPC5 deficiency leads to severe early-onset systemic inflammation and mortality. *Dis Model Mech* 16

Smith BA, Padrick SB, Doolittle LK, Daugherty-Clarke K, Correa IR, Jr., Xu MQ, Goode BL, Rosen
655 MK, Gelles J (2013) Three-color single molecule imaging shows WASP detachment from Arp2/3 complex triggers actin filament branch formation. *Elife* 2: e01008

Somech R, Lev A, Lee YN, Simon AJ, Barel O, Schiby G, Avivi C, Barshack I, Rhodes M, Yin J *et al* (2017) Disruption of Thrombocyte and T Lymphocyte Development by a Mutation in
660 ARPC1B. *J Immunol* 199: 4036-4045

Spudich JA, Watt S (1971) The regulation of rabbit skeletal muscle contraction. I. Biochemical studies of the interaction of the tropomyosin-troponin complex with actin and the proteolytic fragments of myosin. *J Biol Chem* 246: 4866-4871

665

Volpi S, Cicalese MP, Tuijnenburg P, Tool ATJ, Cuadrado E, Abu-Halaweh M, Ahanchian H, Alzyoud R, Akdemir ZC, Barzaghi F *et al* (2019) A combined immunodeficiency with severe infections, inflammation, and allergy caused by ARPC1B deficiency. *J Allergy Clin Immunol* 143: 2296-2299

von Loeffelholz O, Purkiss A, Cao L, Kjaer S, Kogata N, Romet-Lemonne G, Way M, Moores CA (2020) Cryo-EM of human Arp2/3 complexes provides structural insights into actin nucleation modulation by ARPC5 isoforms. *Biol Open* 9

Wagner AR, Luan Q, Liu SL, Nolen BJ (2013) Dip1 defines a class of Arp2/3 complex activators that function without preformed actin filaments. *Curr Biol* 23: 1990-1998

Welch MD, DePace AH, Verma S, Iwamatsu A, Mitchison TJ (1997) The human Arp2/3 complex is composed of evolutionarily conserved subunits and is localized to cellular regions of dynamic actin filament assembly. *J Cell Biol* 138: 375-384

Wu C, Asokan SB, Berginski ME, Haynes EM, Sharpless NE, Griffith JD, Gomez SM, Bear JE (2012) Arp2/3 is critical for lamellipodia and response to extracellular matrix cues but is dispensable for chemotaxis. *Cell* 148: 973-987

Wu C, Orozco C, Boyer J, Leglise M, Goodale J, Batalov S, Hodge CL, Haase J, Janes J, Huss JW, 3rd *et al* (2009) BioGPS: an extensible and customizable portal for querying and organizing gene annotation resources. *Genome Biol* 10: R130

Yamagishi Y, Oya K, Matsuura A, Abe H (2018) Use of CK-548 and CK-869 as Arp2/3 complex inhibitors directly suppresses microtubule assembly both in vitro and in vivo. *Biochem Biophys Res Commun* 496: 834-839

Yang Q, Zhang XF, Pollard TD, Forscher P (2012) Arp2/3 complex-dependent actin networks constrain myosin II function in driving retrograde actin flow. *J Cell Biol* 197: 939-956

Yoon YJ, Han YM, Choi J, Lee YJ, Yun J, Lee SK, Lee CW, Kang JS, Chi SW, Moon JH *et al* (2019) Benproperine, an ARPC2 inhibitor, suppresses cancer cell migration and tumor metastasis. *Biochem Pharmacol* 163: 46-59

Zimmet A, Van Eeuwen T, Boczkowska M, Rebowski G, Murakami K, Dominguez R (2020) Cryo-EM structure of NPF-bound human Arp2/3 complex and activation mechanism. *Sci Adv* 6

Figure Legends

Figure 1. CK-869, but not CK-666 inhibits vaccinia virus-directed actin polymerisation.

A. Representative immunofluorescence image of a HeLa cell infected with vaccinia virus at 9 hours post-infection and labelled with an antibody against cortactin and stained with phalloidin to visualize F-actin. Extra-cellular virus attached to plasma membrane are labelled with an antibody against the viral protein B5. Scale bar = 10 μm. **B.** Representative images showing localization of cortactin in HeLa cells infected with vaccinia at 9 hours post-infection after 1 hour treatment with CK-666 or CK-869 at the specified concentrations. Scale bar = 10 μm. The inset colour images show 2x magnifications of the yellow boxed regions with cortactin (green) and extra-cellular virus (magenta). **C.** The graph shows quantification of the mean number of extracellular virus co-localising with cortactin from three independent repeats with the error bar representing standard deviation. Two tailed unpaired t-test was used to analyse the statistical significance. ns = p-value > 0.05. * = p-value < 0.05. **** = p-value < 0.0001.

Figure 2. CK-666 does not inhibit ArpC1B containing Arp2/3 complexes.

A. Representative plots showing the polymerization of pyrene labelled actin (Fluorescence Intensity) when Arp2/3 iso-complexes containing ArpC1B/C5 (left) or ArpC1B/C5L (right) are activated by GST-N-WASP-VCA in the absence (blue) or presence of 100 μM CK-666 (yellow) or CK-869 (green). **B.** Left shows representative TIRF images showing mother filaments (magenta) and new daughter branches (cyan) 2 minutes after Arp2/3 iso-complexes containing ArpC1B/C5 (top row) or ArpC1B/C5L (bottom row) were activated by GST-N-WASP-VCA in the absence (DMSO) or presence of 100 μM CK-666 or CK-869. Scale bar = 5 μm. The right graph shows the quantification of the mean branching rate for each condition from three independent experiments with the error bar representing standard deviation. Two tailed paired t-test has been applied to analyse the statistical significance. * = p-value < 0.05. *** = p-value < 0.001. ns = p > 0.05.

Figure 3. CK-666 and CK-869 both inhibit ArpC1A containing Arp2/3 complexes

A. Representative plots showing the polymerization of pyrene labelled actin (Fluorescence Intensity) when Arp2/3 iso-complexes containing ArpC1A/C5 (left) or ArpC1A/C5L (right) are activated by GST-N-WASP-VCA in the absence (blue) or presence of 100 μM CK-666 (yellow) or CK-869 (green). **B.** Left shows representative TIRF images showing mother filaments (magenta) and new daughter branches (cyan) 2 minutes after Arp2/3 iso-complexes containing ArpC1A/C5 (top row) or ArpC1A/C5L (bottom row) were activated by GST-N-WASP-VCA in the absence (DMSO) or presence of 100 μM CK-666 or CK-869. Scale bar = 5 μm. The right graph shows the quantification of the mean branching rate for each condition from three independent experiments with the error bar representing standard deviation. Two tailed paired t-test was used to analyse the statistical significance. * = p-value < 0.05. ** = p-value < 0.01.

Figure 4. CK666 has no adverse impact on murine bone marrow-derived macrophages

A. Treatment of murine bone marrow-derived macrophages (BMDM) with 100 μM CK-869 but not DMSO or CK-666 induces cell rounding. The graphs show the mean ratio of length and width as well as cell thickness from five independent experiments with error bars representing the standard deviation. Two tailed unpaired t-test was used to analyse the statistical significance. **B.** Representative phase images of BMDM treated with DMSO, CK-666 or CK-869 over 20 minutes. Scale bar = 20 μm. **C.** Quantification of the mean migration speed of BMDM treated with DMSO, CK-666 or CK-869 from five independent experiments with error bars representing the standard deviation. Two tailed unpaired t-test was used to analyse the statistical significance. **D**. The graph shows the quantification of the phagocytosis efficiency of zymosan by murine bone marrow-derived macrophages treated with DMSO, CK-666 or CK-869 over 120 minutes. Each point represents the mean of three independent technical repeats and error bars represent the standard deviation. Two-way ANOVA test has been applied to analyse the statistical significance. ** = p-value < 0.01. *** = p-value < 0.001. **** means p-value < 0.0001. ns = p > 0.05.

Figure 5. Analysis of Arp2/3 complex binding to actin filaments or the VCA of N-WASP

A. Representative Coomassie stained protein gels showing the co-sedimentation of Arp2/3 complexes containing ArpC1A (left) or ArpC1B (right) with actin filaments (P = pellet) in the absence (DMSO) or presence of 100 μM CK-666 or CK-869. The supernatant (S) contains unbound Arp2/3 complexes and non-pelleted G-actin. MK represents the molecular weight markers. **B.** Quantification of the mean co-sedimentation fraction of the indicated Arp2/3 complexes in the absence (DMSO) or presence of CK-666 or CK-869 from three independent experiments, with the error bars indicating the standard deviation. Two tailed paired t-test was

770 used to analyse the statistical significance. * = p-value < 0.05. ns = p-value > 0.05. **C.** Immunoblots using an ArpC2 antibody demonstrate that 100 μM CK-666 or CK-869 does not impact the interaction of Arp2/3 complexes containing ArpC1A (top) or ArpC1B (bottom) with GST-N-WASP-VCA (Ponceau - red).

775 **Figure 6. The impact of CK-666 and CK-869 on SPIN90 activation of Arp2/3 complexes**
A. Representative plots showing the polymerization of pyrene actin (Fluorescence Intensity) when Arp2/3 complexes containing ArpC1A/C5L (left) or ArpC1B/C5L (right) are activated by SPIN90-Cter in the absence (blue) or presence of 100 μM CK-666 (yellow) or CK-869 (green). **B.** Left shows representative TIRF images of actin filament assembly induced by Arp2/3
780 complexes containing ArpC1A/C5L or ArpC1B/C5L after activation by SPIN90-Cter in the absence (DMSO) or presence of 100 μM CK-666 or CK-869 at the indicated times. Scale bar = 10 μm. The right graph shows the quantification of the mean filament density at 240 s from three independent experiments with the error bar representing standard deviation. Two tailed unpaired t-test was used to analyse the statistical significance and *** = p-value < 0.001. **C.**
785 The left panels show immunoblots of GST-SPIN90-Cter (Ponceau - red) pulldown assays of the indicated Arp2/3 iso-complexes (detected by ArpC2 antibody) in the absence (DMSO) or presence of 100 μM CK-666 or CK-869. The right panel shows the quantification of the mean bound Arp2/3 complex normalized to the DMSO control for three independent pulldown assays with the error bar representing standard deviation. Two tailed paired t-test was used
790 to analyse the statistical significance. ns = p-value > 0.5. * = p-value < 0.5.

Figure 7. Impacts of drugs on Arp3B containing complexes
A Left shows representative TIRF images showing mother filaments (magenta) and new daughter branches (cyan) 2 minutes after Arp2/3 iso-complexes containing
795 Arp3B/ArpC1B/C5L were activated by GST-N-WASP-VCA in the absence (DMSO) or presence of 100 μM CK-666 or CK-869. Scale bar = 5 μm. The right graph shows the quantification of the mean branching rate for each condition from three independent experiments with the error bar representing standard deviation. Two tailed paired t-test was used to analyse the statistical significance and ns = p-value > 0.05. **B.** Left shows
800 representative TIRF images of actin filament assembly induced by Arp2/3 complexes containing Arp3B/ArpC1B/C5L after activation by SPIN90-Cter in the absence (DMSO) or presence of 100 μM CK-666 or CK-869 at the indicated times. Scale bar = 10 μm. The right graph shows the quantification of the mean filament density at 240 s from three independent experiments with the error bar representing standard deviation. Two tailed unpaired t-test was
805 used to analyse the statistical significance. ns means p-value > 0.05. *** presents p-value < 0.001. **C**. The left image shows that in the Arp2/3 complex (PDB: 3ULE), CK-869 has

hydrophobic interactions with Leu 112 and Thr 126 of Arp3. The right image shows that in Arp3B, Leu 112 and Thr 126 are replaced by Met 112 and Leu 126, the latter of which is predicted to have clashes with CK-869.

810

Supplementary Figure Legends

Figure S1. Coomassie stained protein gels of the recombinant proteins and Arp2/3 iso-complexes used in our study.

815

Figure S2. Representative FACS plots of murine bone marrow-derived macrophages phagocytosis under different treatments.

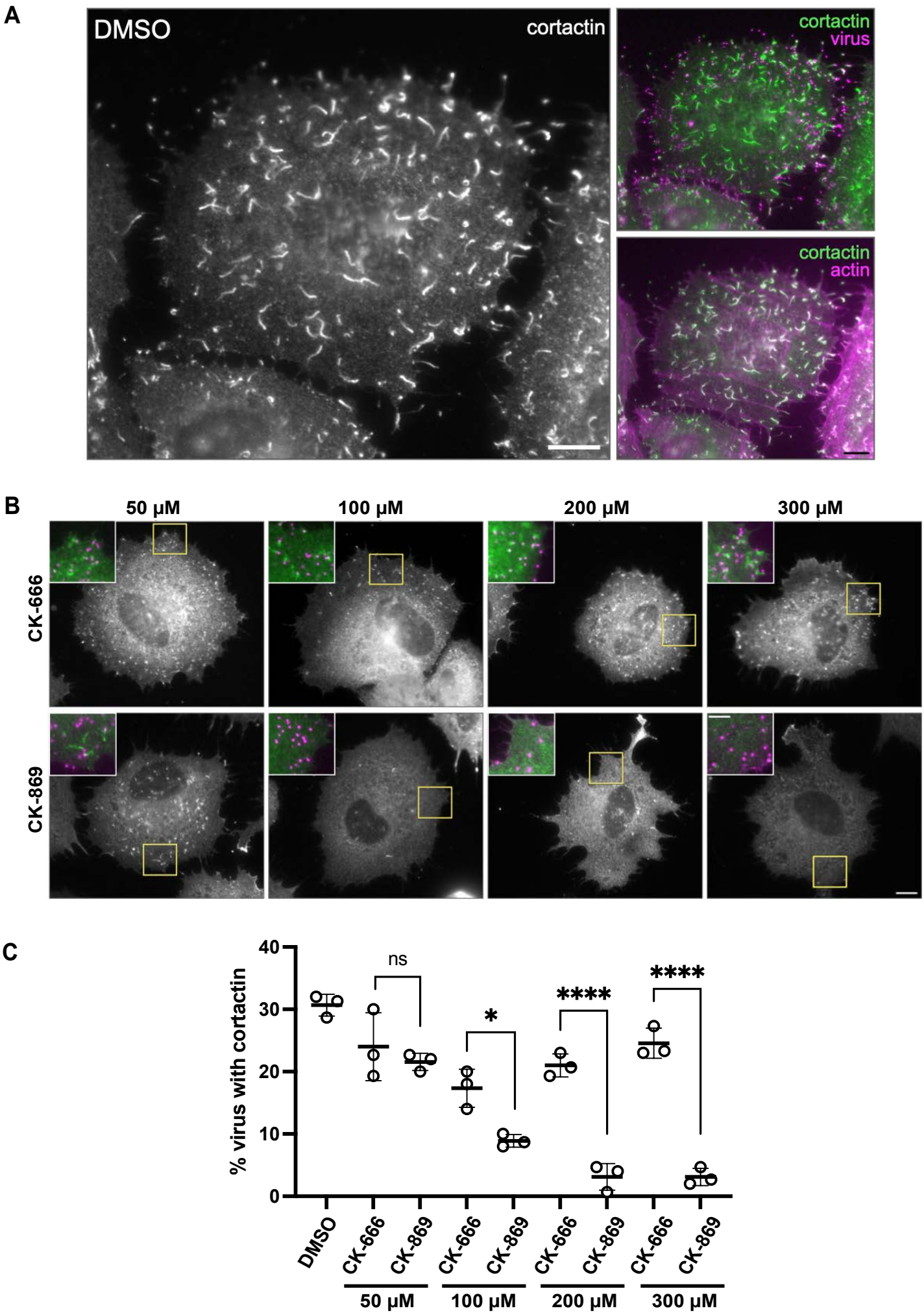
A
DMSO
cortactin
cortactin
virus
cortactin
actin
B
50 µM
100 µM
200 µM
300 µM
CK-666
CK-869
C
% virus with cortactin
40
30
20
10
0
ns
*
****
****
DMSO
CK-666
CK-869
CK-666
CK-869
CK-666
CK-869
CK-666
CK-869
50 µM
100 µM
200 µM
300 µM

Figure 1

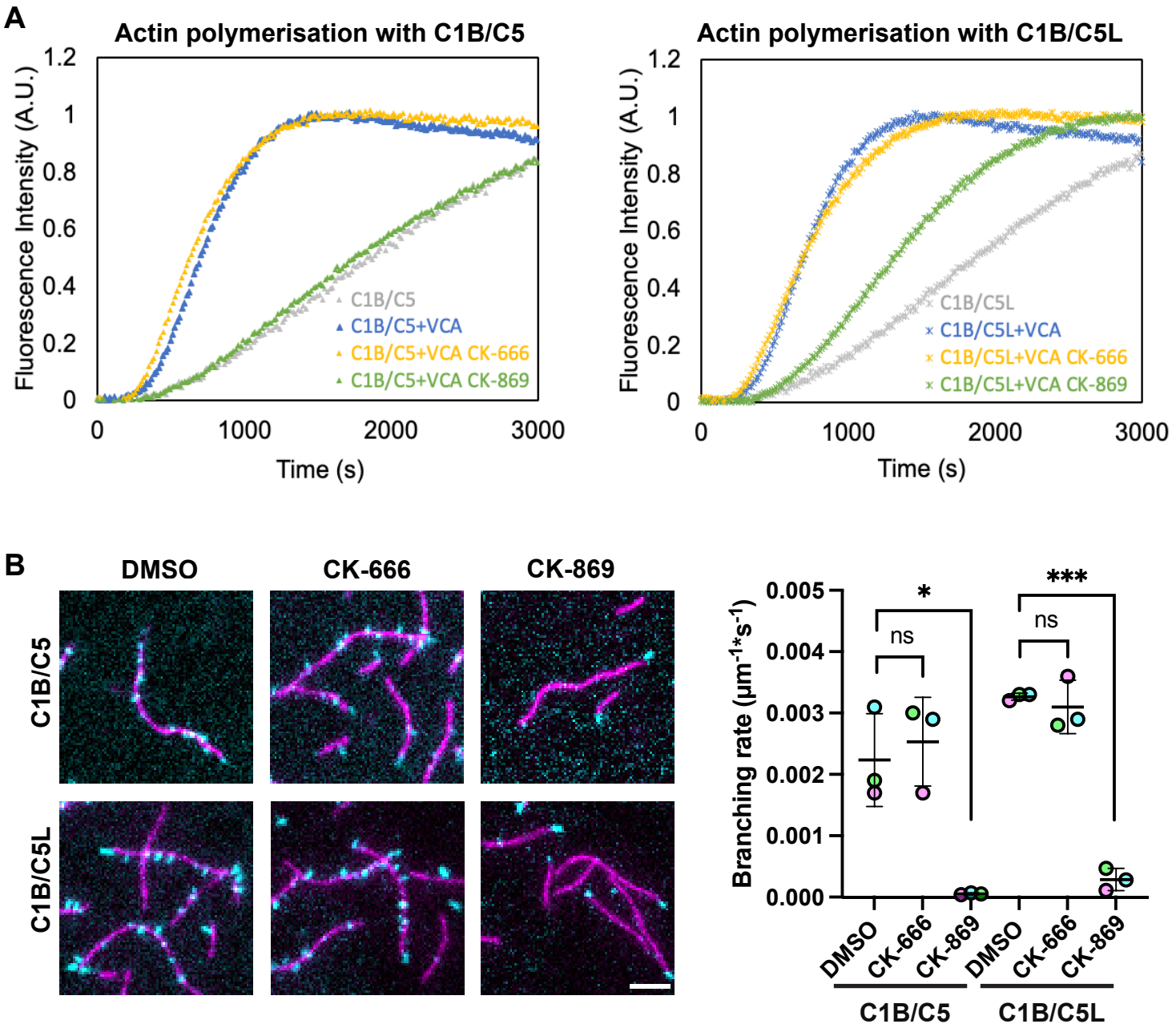
A
Actin polymerisation with C1B/C5
Fluorescence Intensity (A.U.)
Time (s)
C1B/C5
C1B/C5+VCA
C1B/C5+VCA CK-666
C1B/C5+VCA CK-869
Actin polymerisation with C1B/C5L
C1B/C5L
C1B/C5L+VCA
C1B/C5L+VCA CK-666
C1B/C5L+VCA CK-869
B
DMSO
CK-666
CK-869
C1B/C5
C1B/C5L
Branching rate (µm-1*s-1)
ns
*
***
C1B/C5
C1B/C5L

Figure 2

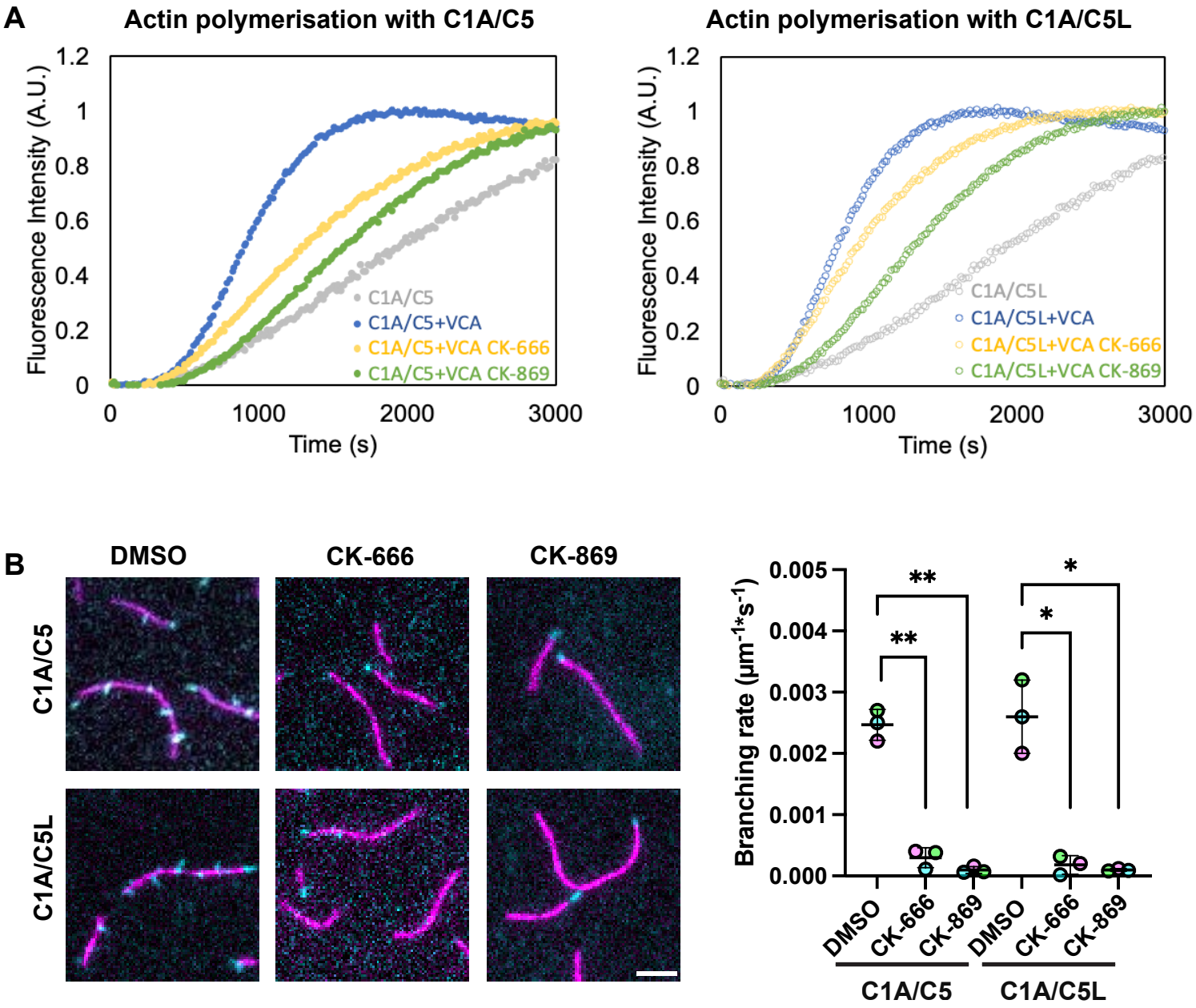
A
Actin polymerisation with C1A/C5
Fluorescence Intensity (A.U.)
Time (s)
C1A/C5
C1A/C5+VCA
C1A/C5+VCA CK-666
C1A/C5+VCA CK-869
Actin polymerisation with C1A/C5L
C1A/C5L
C1A/C5L+VCA
C1A/C5L+VCA CK-666
C1A/C5L+VCA CK-869
B
DMSO
CK-666
CK-869
C1A/C5
C1A/C5L
Branching rate (µm-1*s-1)
DMSO
CK-666
CK-869
C1A/C5
C1A/C5L

Figure 3

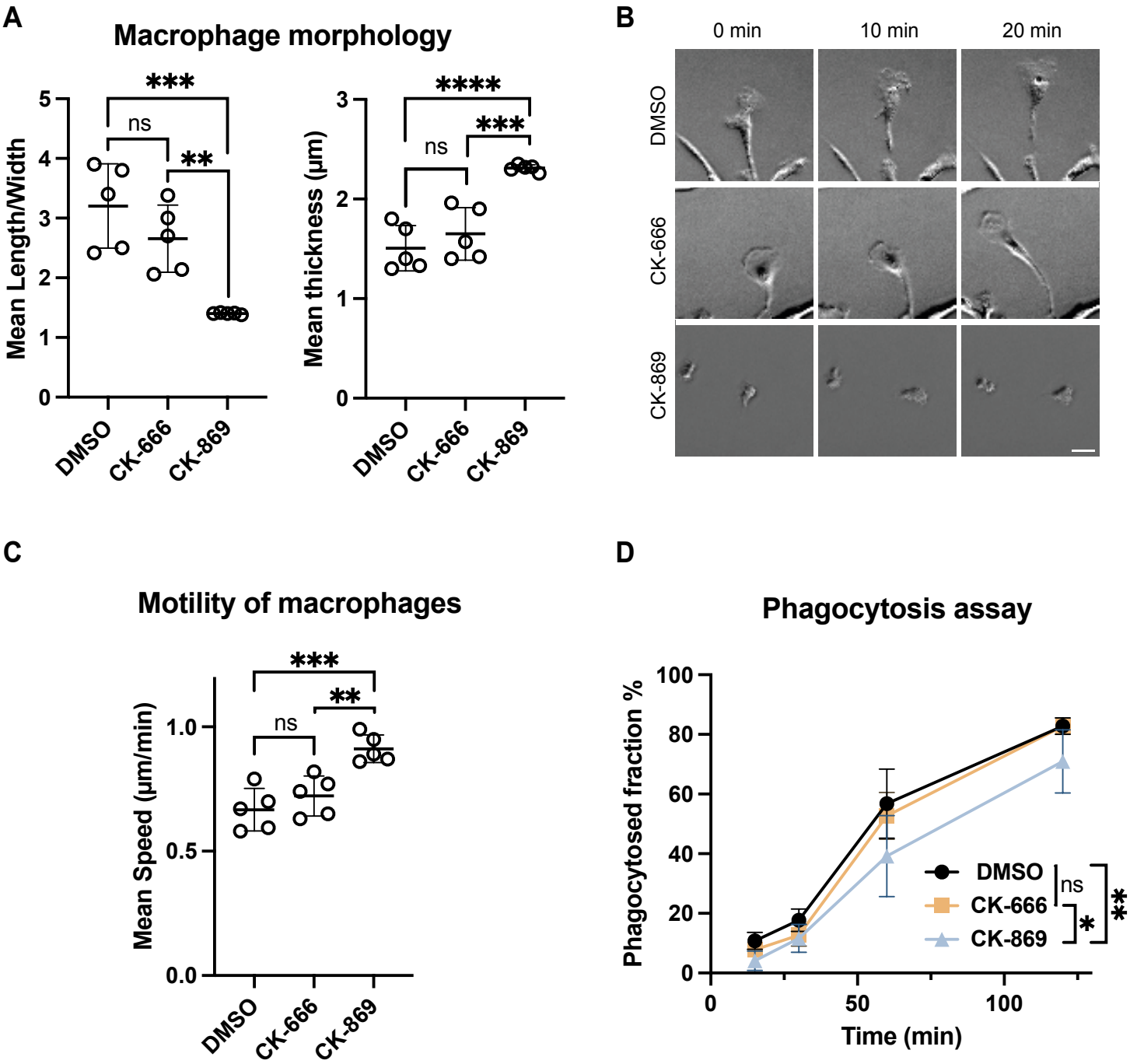
A
Macrophage morphology
Mean Length/Width
***
ns
**
DMSO
CK-666
CK-869
Mean thickness (µm)
****
***
ns
B
0 min
10 min
20 min
DMSO
CK-666
CK-869
C
Motility of macrophages
Mean Speed (µm/min)
***
**
ns
D
Phagocytosis assay
Phagocytosed fraction %
Time (min)
DMSO
CK-666
CK-869
ns
*
**

Figure 4

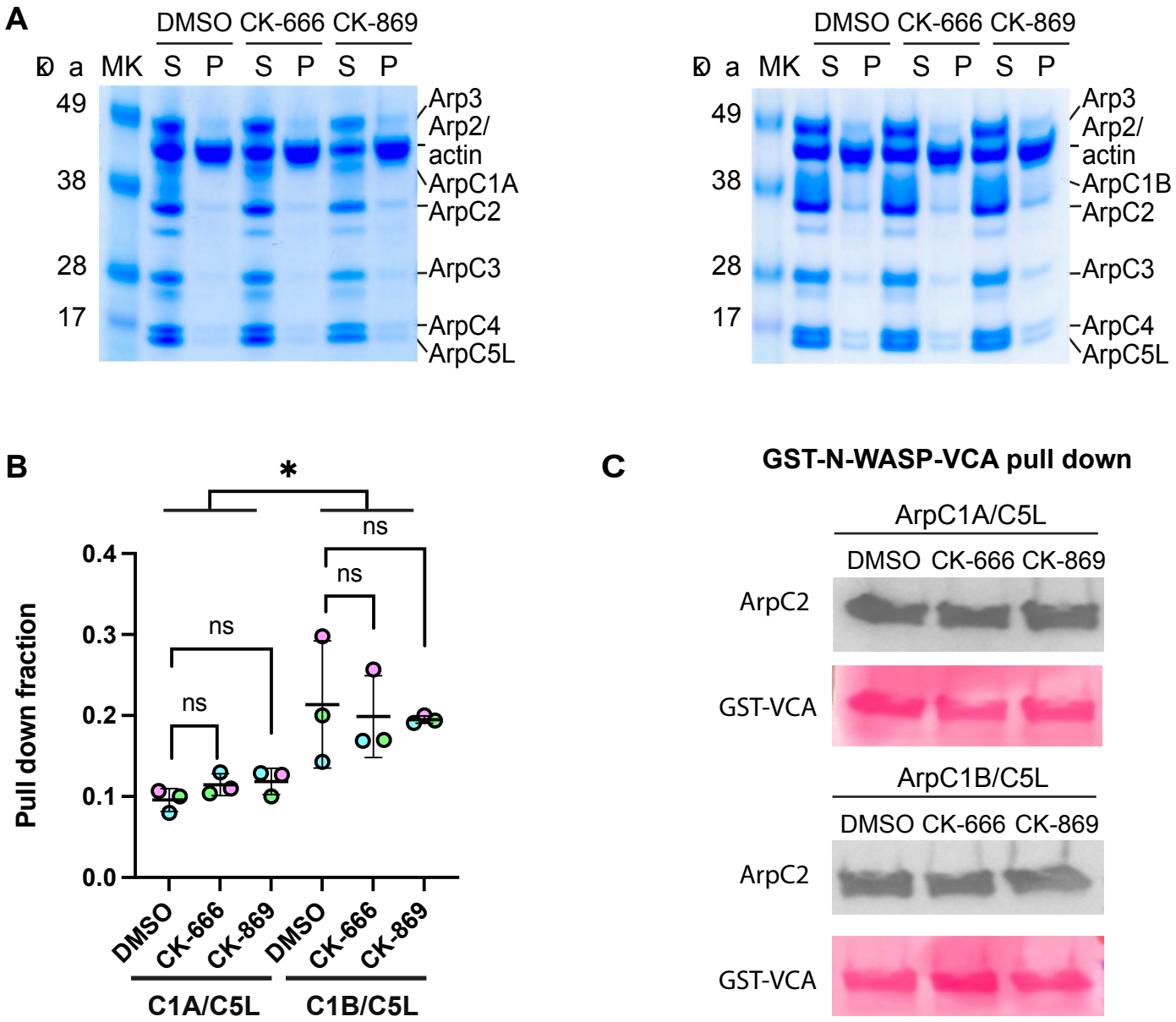
A
DMSO CK-666 CK-869
MK S P S P S P
49
38
28
17
Arp3
Arp2/
actin
ArpC1A
ArpC2
ArpC3
ArpC4
ArpC5L
DMSO CK-666 CK-869
MK S P S P S P
49
38
28
17
Arp3
Arp2/
actin
ArpC1B
ArpC2
ArpC3
ArpC4
ArpC5L
B
*
ns
ns
ns
ns
Pull down fraction
0.4
0.3
0.2
0.1
0.0
DMSO
CK-666
CK-869
DMSO
CK-666
CK-869
C1A/C5L
C1B/C5L
C
GST-N-WASP-VCA pull down
ArpC1A/C5L
DMSO CK-666 CK-869
ArpC2
GST-VCA
ArpC1B/C5L
DMSO CK-666 CK-869
ArpC2
GST-VCA

Figure 5

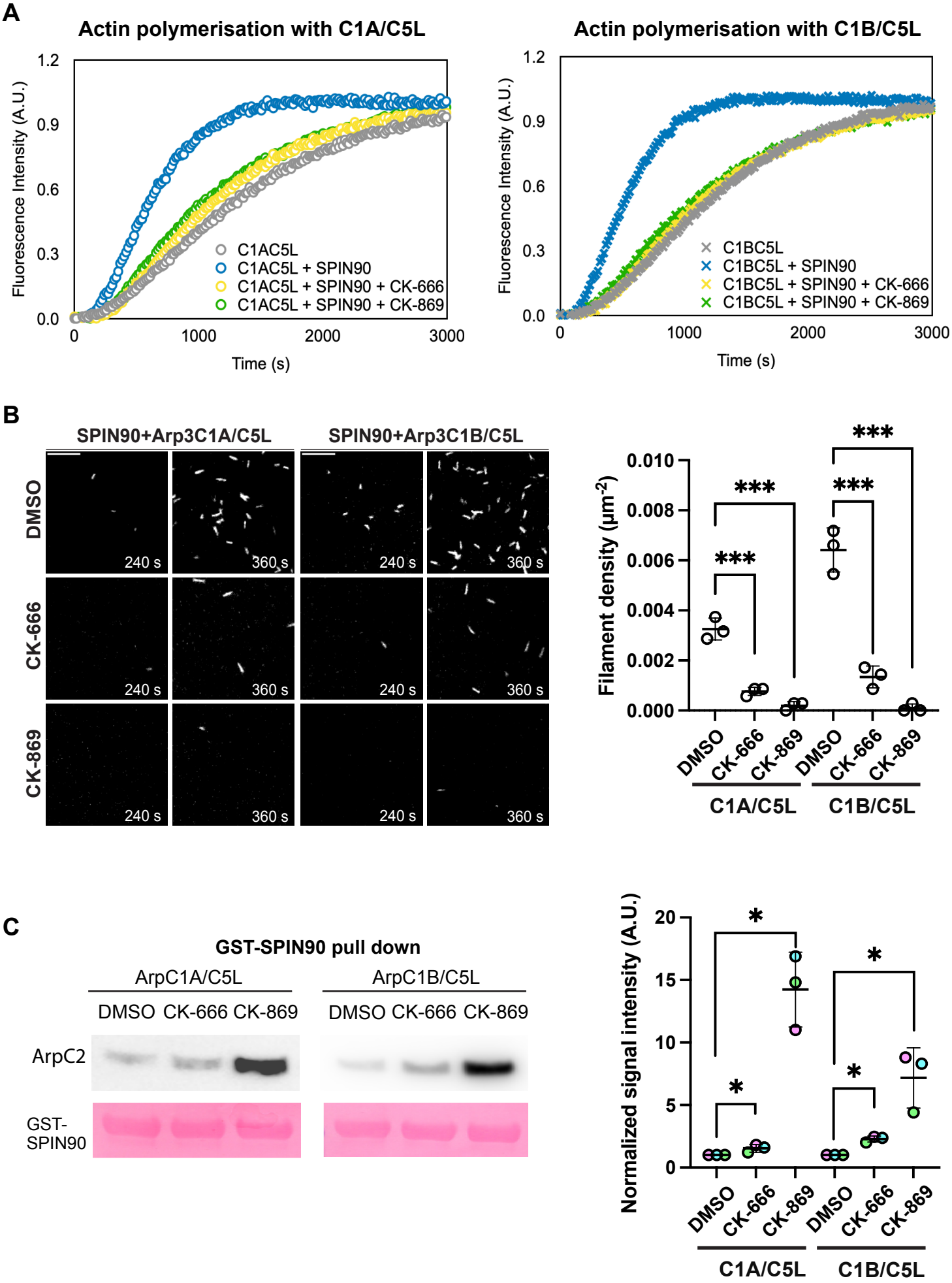
A
Actin polymerisation with C1A/C5L
Fluorescence Intensity (A.U.)
Time (s)
C1AC5L
C1AC5L + SPIN90
C1AC5L + SPIN90 + CK-666
C1AC5L + SPIN90 + CK-869
Actin polymerisation with C1B/C5L
C1BC5L
C1BC5L + SPIN90
C1BC5L + SPIN90 + CK-666
C1BC5L + SPIN90 + CK-869
B
SPIN90+Arp3C1A/C5L
SPIN90+Arp3C1B/C5L
DMSO
CK-666
CK-869
240 s
360 s
Filament density (µm-2)
C1A/C5L
C1B/C5L
C
GST-SPIN90 pull down
ArpC1A/C5L
ArpC1B/C5L
DMSO CK-666 CK-869
ArpC2
GST-SPIN90
Normalized signal intensity (A.U.)

Figure 6

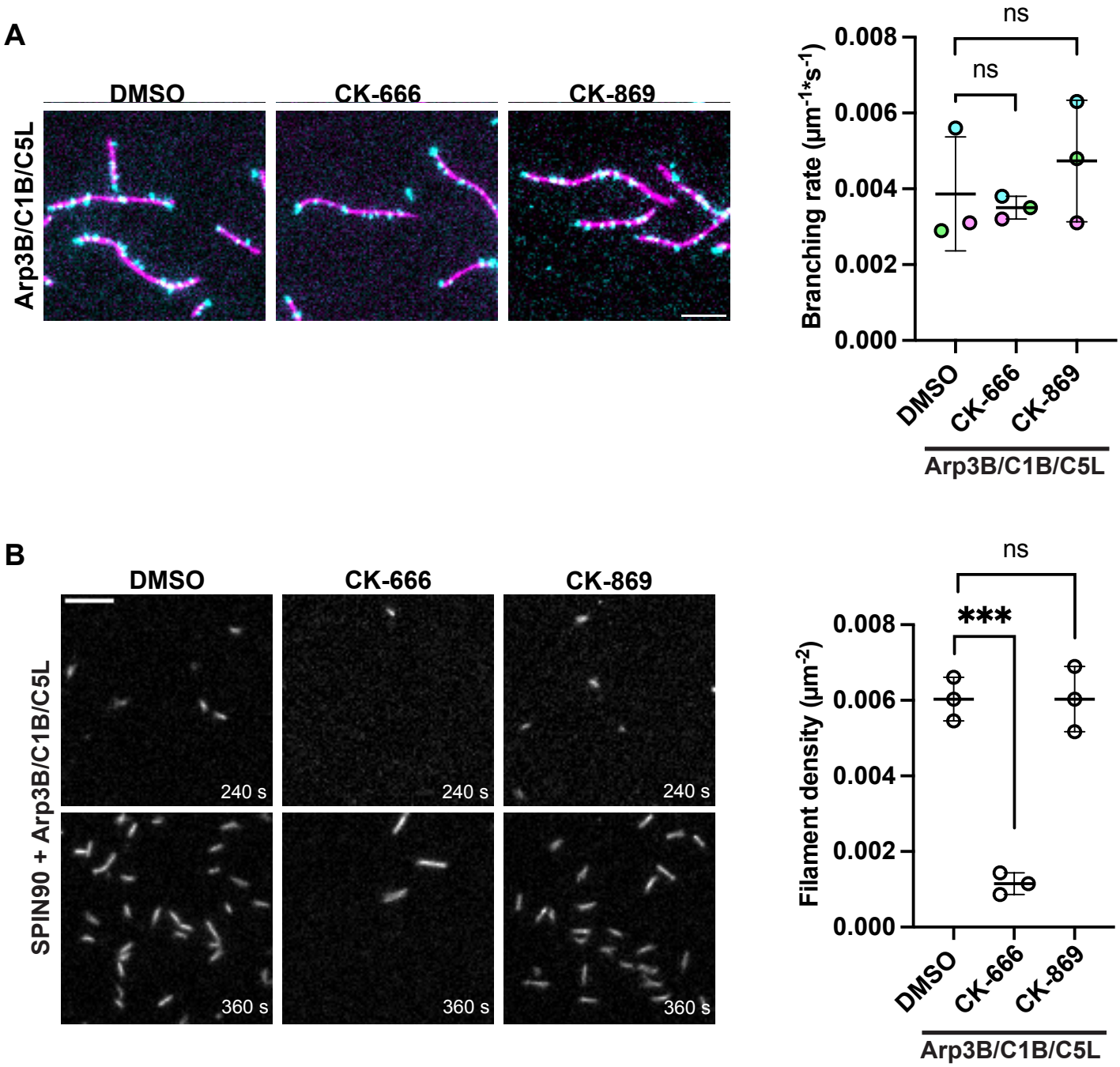
A
DMSO
CK-666
CK-869
Arp3B/C1B/C5L
ns
ns
Branching rate (µm-1*s-1)
0.008
0.006
0.004
0.002
0.000
DMSO
CK-666
CK-869
Arp3B/C1B/C5L
B
DMSO
CK-666
CK-869
SPIN90 + Arp3B/C1B/C5L
240 s
360 s
ns
***
Filament density (µm-2)
0.008
0.006
0.004
0.002
0.000
DMSO
CK-666
CK-869
Arp3B/C1B/C5L

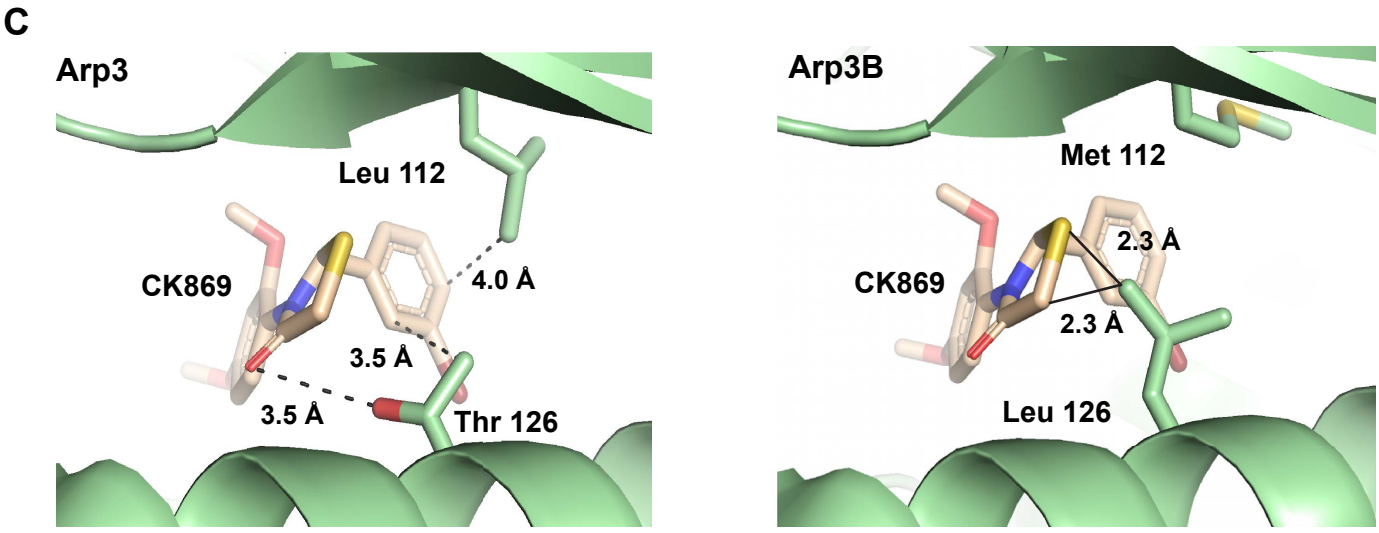
C
Arp3
Leu 112
CK869
4.0 Å
3.5 Å
3.5 Å
Thr 126
Arp3B
Met 112
2.3 Å
CK869
2.3 Å
Leu 126

Figure 7